Towards 2D/3D Registration of the Preoperative MRI to Intraoperative Fluoroscopic Images for Visualization of Bone Defects

Ping-Cheng Ku[a,b], ✉, Alejandro Martin-Gomez[a,b], Cong Gao[a,b], Robert Grupp[a,b], Simon Mears[d], Mehran Armand[a,b,c]

[a]Biomechanical- and Image-Guided Surgical Systems (BIGSS), Laboratory for Computational Sensing and Robotics, Johns Hopkins University, Baltimore, MD, USA
[b]Department of Computer Science, Johns Hopkins University, Baltimore, MD, USA
[c]Department of Orthopaedic Surgery, Johns Hopkins University, Baltimore, MD, USA
[d]Department of Orthopaedic Surgery, University of Arkansas for Medical Sciences, AR, USA

ABSTRACT

Magnetic Resonance Imaging (MRI) is a medical imaging modality that allows for the evaluation of soft-tissue diseases and the assessment of bone quality. Preoperative MRI volumes are used by surgeons to identify defected bones, perform the segmentation of lesions, and generate surgical plans before the surgery. Nevertheless, conventional intraoperative imaging modalities such as fluoroscopy are less sensitive in detecting potential lesions. In this work, we propose a 2D/3D registration pipeline that aims to register preoperative MRI with intraoperative 2D fluoroscopic images. To showcase the feasibility of our approach, we use the core decompression procedure as a surgical example to perform 2D/3D femur registration. The proposed registration pipeline is evaluated using digitally reconstructed radiographs (DRRs) to simulate the intraoperative fluoroscopic images. The resulting transformation from the registration is later used to create overlays of preoperative MRI annotations and planning data to provide intraoperative visual guidance to surgeons. Our results suggest that the proposed registration pipeline is capable of achieving reasonable transformation between MRI and digitally reconstructed fluoroscopic images for intraoperative visualization applications.

KEYWORDS
2D/3D registration, core decompression, avascular necrosis,

1. Introduction

Magnetic Resonance Imaging (MRI) is an imaging technique that does not require the use of ionizing radiation as the images are produced based on the magnetic properties of tissues rather than their radiodensity. This property has made MRI a good candidate for the evaluation of soft-tissue diseases, the assessment of bone quality, and the detection of bone tumors and tumor-like lesions (Chung et al. 2012; Chang et al. 2017; Nascimento et al. 2014). Nevertheless, traditional intraoperative imaging modalities such as fluoroscopy are less sensitive in detecting soft tissues diseases and bone lesions, which makes surgeries that rely heavily on information from preoperative MRIs challenging (Pierce et al. 2015a).

✉ E-mail: pku1@jhu.edu

A clear example of the lesion that is visible in preoperative MRI but hardly detectable intraoperatively is avascular necrosis (AVN). AVN of the femoral head is a disease that may lead to the collapse of the femoral head and articular disability. Surgical treatments of AVN during the early stages are crucial as they result in better treatment outcomes (Rocchi et al. 2020). The core decompression method is a surgical procedure that creates a drilling hole made from the distal end of the trochanter to stimulate the blood supply to the necrotic area, diminish the femoral head pressure, and delay the progression of osteonecrosis (Lieberman 2004; Yu et al. 2018). Core decompression has become a preferred procedure to treat early-stage AVN due to its simplicity, low complication rate, and promising efficacy (Lieberman 2004; Veillette et al. 2006; Talmaç 2018; Nori 2015). During the surgery, the precision of the drilling is essential to accurately decompress the targeted lesions while avoiding any femoral cartilage damage (Beckmann et al. 2006).

Throughout core decompression surgery, different modalities of medical imaging techniques are involved. MRI is the most sensitive and specific imaging technology for the diagnosis of the early-stage and precollapse-stage AVN as it allows the surgeons to visualize the size and the position of the lesion (Saini and Saifuddin 2004). Intraoperative imaging techniques such as C-arm fluoroscopy or X-ray have become important for the localization of the greater trochanter, tracking and navigation of the drilling and injection device to the femoral head, and positioning of the trephine and scraping spoon while removing the dead bones (Nolte et al. 2000; Geisert et al. 2017; Tian et al. 2021). However, studies have shown that radiographs exhibit low sensitivity for the early stages of AVN; while MRI scans are particularly sensitive to the detection of necrotic tissues, MRI scans are hard to acquire intraoperatively (Malizos et al. 2007). As a result, the outcome of the procedure often relies on the surgeons' past experience and their ability to generate three-dimensional representations from a collection of two-dimensional images. Core decompression procedure requires the acquisition of multiple intraoperative radiographs, which increases the risk of surgical complications and increases the radiation exposure for both the patient and the surgical team (Beckmann et al. 2006; Wang et al. 2017).

Since the lesion segmentation and the planning of drilling paths are carried out using preoperative MRI, being able to visualize these pre-operative annotations during surgery is a potential solution to this situation. This involves a 2D/3D registration problem between pre-operative MRI and 2D intraoperative radiographs. Nevertheless, direct automatic registration between MRI volumes and 2D radiography such as X-rays and C-arm fluoroscopy has been a challenging task, as the differences in their imaging physics and contrast mechanisms lead to varying tissue contrasts (van der Bom et al. 2011).

2. Related Work

In this paper, we propose a novel 2D/3D registration pipeline that aims to register preoperative MRI and intraoperative fluoroscopic images without the requirement of preoperative CT scans from the patient. The proposed registration pipeline includes two main steps, including the MR-to-CT synthesis and the 2D/3D registration process.

2.1. MR-to-CT synthesis

The challenge of MRI to 2D radiograph registration lies in the mismatched image intensities and anatomical structure correspondence. Recently, the development of learning-based algorithms allows the estimation of non-linear mappings between MRI and CT. Self-optimizing algorithms such as random forest (Andreasen et al. 2016) and convolutional neural networks were used to generate synthetic CT of pelvis from MRI (Leynes et al. 2017).

As MR-to-CT synthesis could be considered a style-transfer problem, algorithms based on Generative Adversarial Net (GAN) and its variants have been utilized to perform cross-modality image synthesis in medical images (Nie et al. 2018; Brou Boni et al. 2020). These algorithms train one or more generator and discriminator networks simultaneously (Goodfellow et al. 2014) to create high-quality synthesized CT from MRI images.

The introduction of Cycle-Consistent Adversarial Network (CycleGAN) has made significant progress in medical image synthesis (Zhu et al. 2017) since the network does not require paired or registered images for training, which are generally hard to acquire. CycleGAN-based frameworks have been used in MR-to-CT synthesis for different anatomical structures (Fu et al. 2020; Kalantar et al. 2021). However, performing MR-to-CT synthesis through the naive CycleGAN often results in inconsistent structures between input and synthetic images. To avoid geometric distortions, additional loss functions such as gradient consistency loss (Hiasa et al. 2018) and structure-consistency loss (Yang et al. 2020) have shown promising results.

2.2. 2D/3D registration

Performing a 2D/3D registration between preoperative volumes and intraoperative projection image has made significant improvements to orthopedic surgeries (Zhang et al. 2006). A good registration between different imaging modalities allows the surgeons to monitor various anatomy, enables computer-assisted navigation algorithms for additional guidance during surgery, and may reduce the number of scans required to perform the procedure.

The goal of 2D/3D registration is to determine the pose of 3D objects with respect to a 3D coordinate frame using a series of 2D images. The 3D models are typically preoperative CT volumes and the 2D images are usually intraoperative radiographs such as X-ray or C-Arm fluoroscopic images. Registration pipelines between CT and 2D radiographs have been proposed for surgical treatments around the hip region such as periacetabular osteotomy (Grupp et al. 2020) and femoroplasty (Gao et al. 2020).

However, the 2D/3D registration between MRI and 2D intraoperative radiographs has been challenging due to the lack of cross-modality information. The registration between breast MRI and X-ray mammography has shown to be feasible through a properly defined volume-preserving affine transformation model (Mertzanidou et al. 2012) or through gradient-based registration methods (García et al. 2019). Both algorithms are able to reach registration accuracy in the order of 10mm.

Recently, a contour-based approach performs 2D/3D registration between preoperative spine MRI and intraoperative 2D radiographs. The registration error of the study is less than 3mm. Nevertheless, this approach relies heavily on the initial segmentation of the vertebra in pre-operative MRI, which makes this method less robust and less likely to perform well while registering a different anatomical structure.

To our knowledge, there is no research on MRI to 2D radiography registration as a

tool for intraoperative visualization of bone defects. Therefore, the main contributions of this paper include the development of a pipeline for MRI to intraoperative fluoroscopy registration for visualization of bone defects that cannot be directly observed in intraoperative 2D radiographs. The pipeline includes:

(1) Development of a CycleGAN-based network optimized to generate CT from preoperative MRI;
(2) Development of a synthetic CT to X-ray registration method for femur;
(3) Visualization of registration result by superimposing preoperative MRI annotations onto intraoperative 2D images.

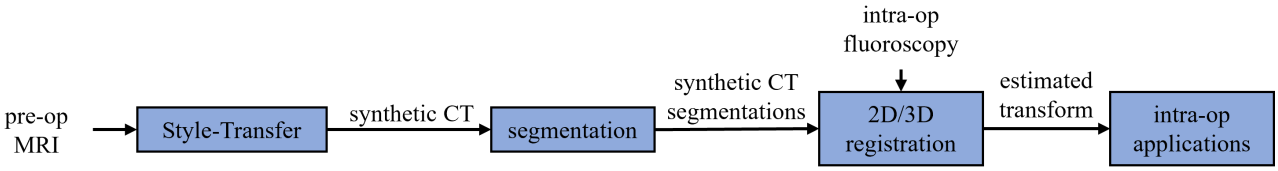

Figure 1.: The proposed 2D/3D registration pipeline to perform registration between preoperative MRI and intraoperative fluoroscopic images.

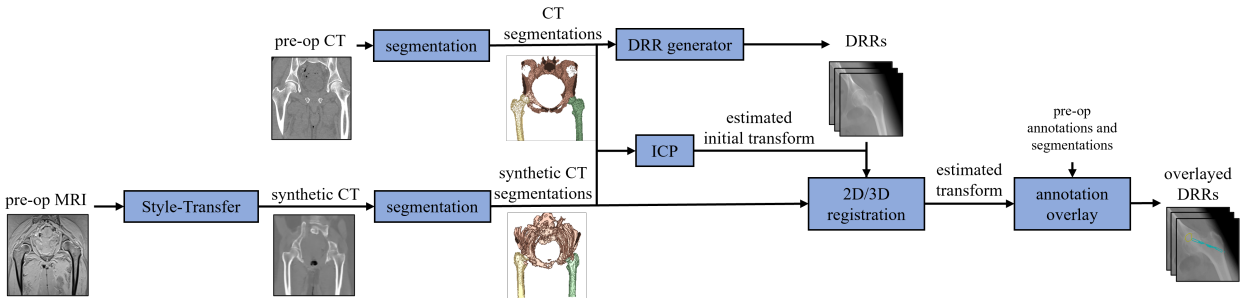

Figure 2.: The 2D/3D registration pipeline for the core decompression procedure in this study, using DRRs as replacement for intraoperative fluoroscopy images.

3. Methods

We propose a MRI to fluoroscopy registration pipeline (see Figure 1), which is as follow: (1) generation of synthetic CT (sCT) volumes from MRI, (2) segmentation of synthetic CT, (3) 2D/3D registration between synthetic CT and intraoperative fluoroscopic images, (4) intraoperative applications and assessments.

In this paper, we use the core decompression procedure as a surgical example for the proposed pipeline. Due to the limited access to intraoperative radiographs, instead of fluoroscopic images, digitally reconstructed radiographs (DRRs) from the paired real CT (rCT) scans are used. Visual representation of pre-operative annotations and segmentations are selected as the intraoperative application for the core decompression procedure study. The 2D/3D registration pipeline between MRI and DRRs for this study is illustrated in Figure 2.

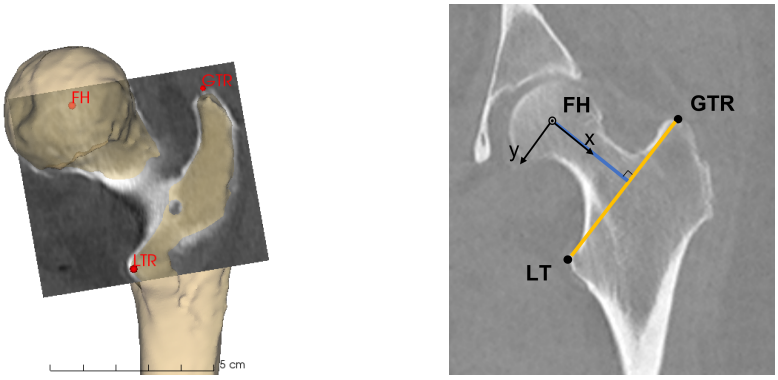

(a) (b)

Figure 3.: Visualization of femoral ACS plane in (a) 3D space, and in (b) CT volume, with the three landmarks GT, FH, GTR annotated.

3.1. Data preparation

The proposed pipeline for the core decompression study requires preoperative MRI and CT volumes from the same patient, and preoperative MRI annotations such as AVN lesion segmentation and core decompression planning device paths. To acquire the initial relative poses between the MRI and CT volumes, reliable methods of determining the local anatomical coordinate system (ACS) is necessary. To construct the femoral ACS, three anatomical landmarks are manually annotated in the CT volumes prior to the experiments: center of the femoral head (FH), the tip of the superoposterior facet of the greater trochanter (GTR), and the tip of lesser trochanter (LTR) (Domb and Carreira 2013). An example of the femoral ACS is shown in Figure 3.

3.2. Generation of synthetic CT from pre-operative MRI

We introduce a style-transfer step in the registration pipeline to generate synthetic CT (sCT) volumes from preoperative MRI volumes. With a trained network model, the generated sCT will detect and preserve the bone structures with high image intensities and reduce the intensity impact of the soft tissues from the input MRI. This paper adopts the modified CycleGAN model proposed by Hiasa et al. which introduces a gradient consistency loss ($\mathcal{L}_{gc}$) in the loss function (Hiasa et al. 2018). The overall cycleGAN loss ($\mathcal{L}$) is defined as:

$$\begin{aligned}\mathcal{L}(G_{CT}, G_{MR}, D_{CT}, D_{MR}) =& \mathcal{L}_{adv}(G_{CT}, D_{CT}) + \mathcal{L}_{adv}(G_{MR}, D_{MR}) + \\ & \lambda_{cyc}\mathcal{L}_{cyc}(G_{CT}, G_{MR}) + \lambda_{gc}\mathcal{L}_{gc}(G_{CT}, G_{MR})\end{aligned}$$

where $\mathcal{L}_{adv}$ is the adversarial loss, λ_{cyc} is the cycle consistency loss, G is the generator network and D is the discriminator network of the CycleGAN. The cycle consistency weight parameter (λ_{cyc}) and gradient consistency weight parameter (λ_{gc}) are used to control the importance of the corresponding loss terms.

In order to accommodate the MRI volume in the CycleGAN model, the following prepossessing steps are performed: (1) set the origin of the MRI DICOM file to the world origin, (2) resample the input MRI volume to a 1mm-isotropic volume, (3) resize the coronal slices into patches with size 256×256. The preprocessing steps above

are modeled as a non-rigid transformation, denoted as $T_{GT_{sCT}}^{GT_{MR}}$, which represents the transformation of the sCT ground truth frame (GT_{sCT}) with respect to the ground truth frame of the MRI volume (GT_{MR}).

Acquiring the transformation between the MRI and sCT volume allows the calculation of the transformation between the MRI space to the 2D radiograph frame space after the 2D/3D registration process is performed in Section 3.4.

3.3. Estimation of initial pose for 2D/3D registration

In this study, DRRs are used as a replacement for intraoperative fluoroscopy images in the proposed pipeline. The generation of DRR creates a realistic simulation of the intraoperative fluoroscopy, and it also enables us to perform a more comprehensive 2D/3D registration analysis with the increased number of projections available in various projecting directions. The DRR images are generated by calculating ray casting line integrals through perspective projections of the 3D CT volumes onto 2D image planes (Grupp et al. 2020). In this work, the default camera pose is positioned along the z-axis of the femoral ACS plane and the camera points towards the patient posterior. Random perturbations will be applied to the camera to generate various DRR projections for registration. The generated DRRs (I_m) are used to simulate intraoperative radiographs and are used in the 2D/3D registration step.

To perform registration between the sCT and the DRRs generated from the rCT volumes, it is critical to ensure that the pose of the femoral head in the sCT is spatially close to the pose of the real patient CT. To reduce the probability of the 2D/3D registration step trapping in local optima, we apply Iterative Closest Point (ICP) algorithm (Rusinkiewicz and Levoy 2001) for better pose initialization.

Let the origin ground truth of the rCT volume be denoted by GT_{rCT} and the femoral ACS be denoted by FH_{rCT}. We denote the ground truth and the femoral ACS of the sCT volume by GT_{sCT} and FH_{sCT}, respectively (see Figure 4). To perform the ICP algorithm, both sCT and rCT volumes are first segmented through the automatic bone segmentation method introduced by Krcah et al. (Krčah et al. 2011). The segmentation created through this method is occasionally followed by manual label adjustments to separate the pelvis acetabulum and the femoral head. After the segmentation of sCT and rCT volumes, the mesh files of the femurs are automatically created. A set of point cloud is then generated around the femoral head of the sCT by randomly selecting a fixed number of vertices from the mesh file of the sCT. The ICP algorithm then optimizes over a rigid transformation by minimizing the summation of the distance between each point and the surface mesh of the rCT volume. The ICP algorithm produces an estimation of the ground truth frame of the sCT with respect to the rCT ($T_{GT_{rCT}}^{GT_{sCT}}$). This transformation is then applied to the entire sCT volume to generate a properly initialized and resampled sCT volume for the 2D/3D registration.

3.4. 2D/3D registration between synthetic CT and fluoroscopic image

In this work, we apply an intensity-based approach to achieve the 2D/3D registration between synthetic CT and DRRs. Intensity-based registration aims to perform an optimization over target pose parameters, using an objective function that compares a sequence of DRRs with the intraoperative image. The registration in this work is

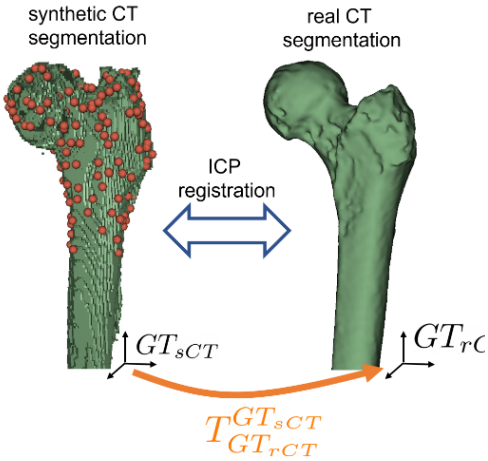

Figure 4.: 3D/3D registration between the synthetic CT segmentation and the real CT segmentation through ICP.

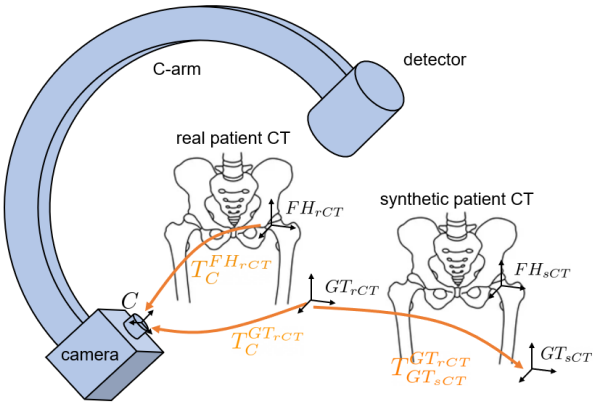

Figure 5.: Visualization of different frame transformations during the 2D/3D registration procedure

solved by optimizing the following optimization problem:

$$\min_{T \in SE(3)} \mathcal{S}(I_m, \sum_{n=1}^{N} \mathcal{P}(V_{CT}; T)) + \mathcal{R}(T) \tag{1}$$

where the V_{CT} represents the input CT volume; $\mathcal{P}$ represents the DRR operator; $\mathcal{S}$ represents the similarity metric used; $\mathcal{R}$ represents a regularizer over plausible poses; and T represents the 3D rigid transformation to be solved between the C-arm camera frame (denoted as C) and a pose of the input CT volume. In this work, this transformation is the one between C-arm camera frame and the ground truth pose of the CT volume $T_C^{GT_{CT}}$, and we denote the registered transformation outcome as $(T_C^{GT_{CT}})_{regi}$.

The normalized gradient cross-correlation (Grad-NCC) method is used to calculate the similarity scores between the image patches (Grupp et al. 2018). The 2D images are cropped and down-sampled 4 times in each dimension. The search algorithm – "Covariance Matrix Adaptation: Evolutionary Search" (CMA-ES) – is selected as the optimizer for our registration task (Hansen et al. 2003).

Since the sCT coordinate is first transformed to the rCT volume frame during the 2D/3D registration initialization, the transformation from the ground truth sCT frame to the C-arm view is calculated by: $(T_C^{GT_{sCT}})_{regi} = (T_{GT_{sCT}}^{GT_{rCT}})^{-1} \cdot (T_C^{GT_{rCT}})_{regi}$. Once the transformation $(T_C^{GT_{CT}})_{regi}$ is acquired after the 2D/3D registration, the transformation between the MRI volume and the DRR could be calculated through:

$$(T_C^{GT_{MR}})_{regi} = T_{GT_{sCT}}^{GT_{MR}} \cdot (T_C^{GT_{sCT}})_{regi} = T_{GT_{sCT}}^{GT_{MR}} \cdot (T_{GT_{sCT}}^{GT_{rCT}})^{-1} \cdot (T_C^{GT_{rCT}})_{regi} \tag{2}$$

The transformation $(T_C^{GT_{MR}})_{regi}$ allows annotations from preoperative MRI volumes to be registered or overlayed onto the DRR images generated from the C-arm camera.

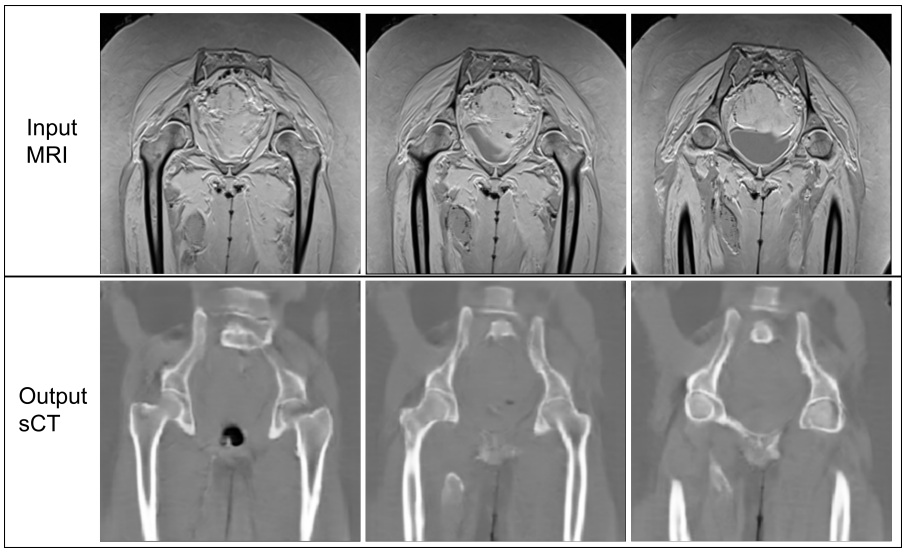

Figure 6.: The result of MR-to-CT image synthesis around the hip area through gradient consistency based CycleGAN network.

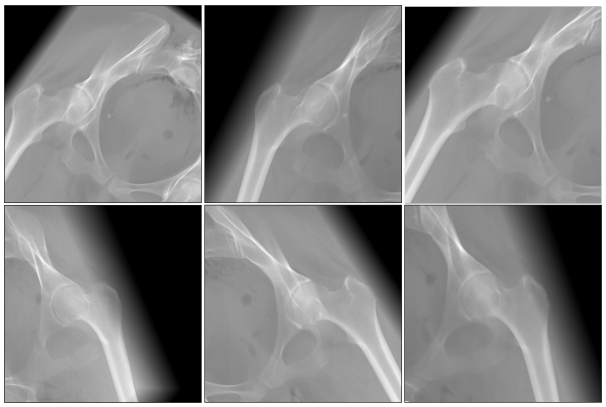

Figure 7.: DRRs from a single patient, used as a replacement of 2D fluoroscopy.

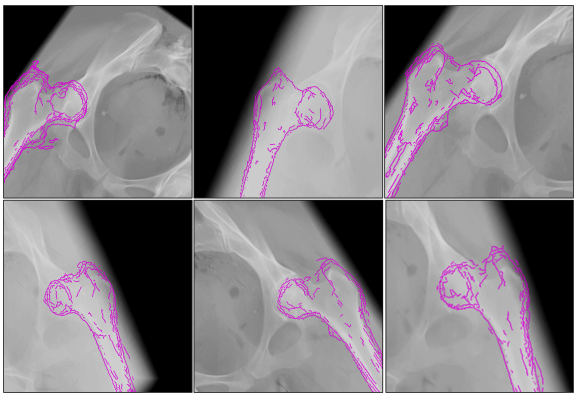

Figure 8.: The singleview registration result with the overlay of femur from sCT.

4. Experiments and results

In this work, three MRI volumes from different patients are acquired. Each volume has a voxel spacing of 1.40 × 1.40 × 1.00 mm. Two volumes have a dimension of 352 × 352 × 192 while the third volume has a dimension of 352 × 352 × 192. A total of three CT volumes are also acquired from the corresponding patients. A total of six anatomical landmarks in each volume are first annotated to define the femoral ACS for both the left and the right femur.

A gradient consistency integrated CycleGAN network is trained in this experiment. The three MRI volumes are used as our MRI dataset; a total of 12 coronal torso CT volumes from the New Mexico Decedent Image Database (NMDID) are used as our CT dataset. The voxel spacing of the CT volumes is 0.68 × 0.68 × 0.5 mm. The CT volumes are cropped to match the field of view of MRI volumes. The cropped volumes have a total of 94 to 152 coronal slices, each with a dimension of 460 × 460.

Data augmentations including random zooming, random spatial cropping, and ran-

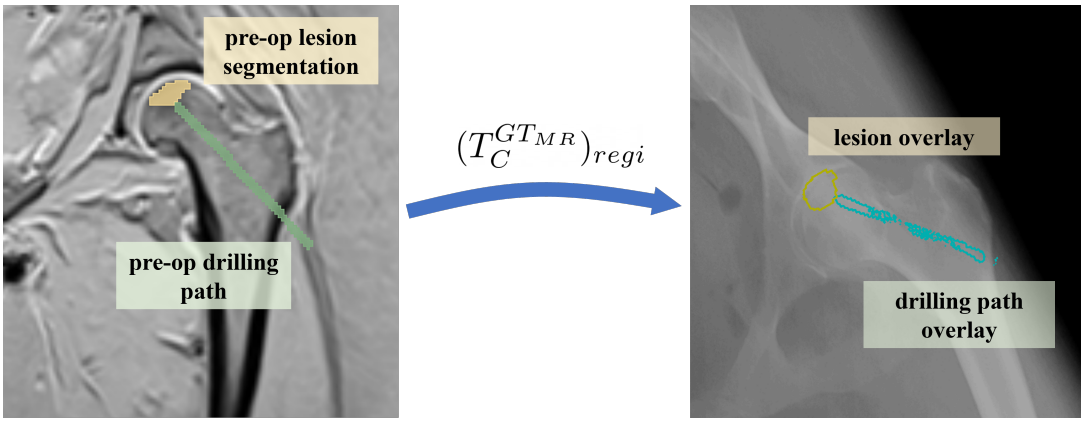

Figure 9.: Left image – AVN lesion segmentation and core decompression drilling paths annotated on preoperative MRI. Right image – annotation overlay on simulated radiogrpah.

dom rotations are performed before the training of the CycleGAN network to compensate for the insufficiency of the MRI volumes that are available. In this study, the gradient consistency loss parameter (λ_{gc}) is empirically set to 0.2 while the cycle-consistency loss parameter ($\mathcal{L}_{cyc}$) is empirically set to 10. The CycleGAN network is trained with 1000 MRI and CT images and for 100 epochs. An example of the network training result is shown in Figure 6. To evaluate the performance of the network quantitatively, the synthesized CT image is compared to ground truth CT using structural similarity image measure (SSIM) and mean squared error (MSE). The ground truth CT is acquired by performing registration through advanced normalization Tools (ANTs) (Avants et al. 2014). The final SSIM result has a mean of 0.3556 and a standard deviation of 0.1238; while the MSE result has a mean of 0.0981 and a standard deviation of 0.0216. The transformations between the input MRI and the sCT ($T_{GT_{sCT}}^{GT_{MR}}$) for all three subjects are calculated and saved.

Once the sCT volumes are generated from the MRI volumes, the sCT and the rCT volumes from the corresponding patient are segmented through the automatic bone segmentation application with some manual touch-up. The C-Arm intrinsic parameter chosen to generate the DRR simulates the projection geometry of a Siemens CIOS Fusion C-Arm. The source to image-receptor distance is 1020 mm, and the image matrix size is 1536 $\times$ 1536 pixels, where the pixel size is 194 μm. For each patient, a total of 10 random camera poses are generated for the left and right femurs. The default camera pose is positioned along the femoral ACS z-axis at a distance of 749mm. To generate random camera poses for this study, we apply a perturbation transformation to the default camera poses, where the perturbation transform includes a random rotation between -5°to 5°and a random translation from -10 to 10 mm in a random direction. This adds up to a total of 60 simulated projections in this study. An example of the generated DRR images is shown in Figure 7.

To acquire the initial registration transform for the sCT to DRR registration, 200 points are selected randomly around the femoral head of the sCT and then rigidly registered to the surface mesh of the rCT. In this work, a total of 60 simulated radiographs with varying camera poses are studied and their registration accuracy with sCT volumes is analyzed. Table 1 shows the result of the registration error for the three subjects. The mean femur registration error is 12.95 $\pm$ 4.90 mm, and the rotation error is 4.51 $\pm$ 2.67 degrees. The translation error in the table is further separated into two components: in-plane error and out-of-plane error. The in-plane error represents the

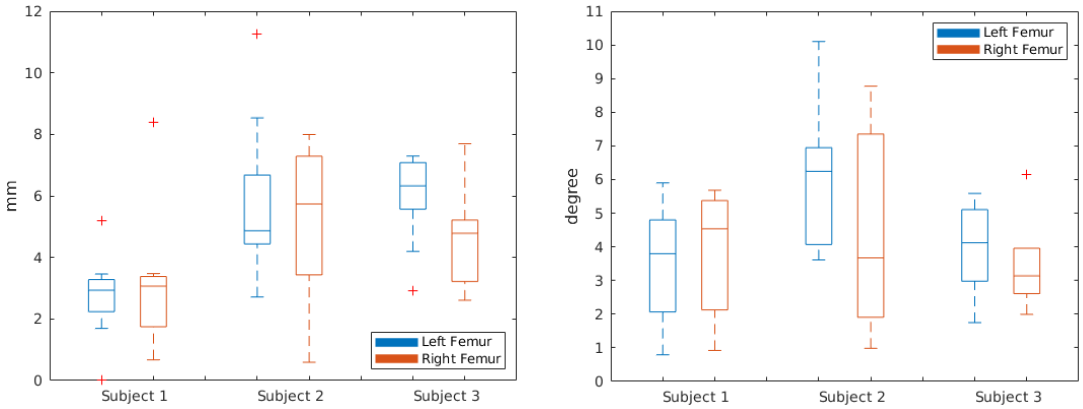

(a) (b)

Figure 10.: Registration errors between sCT and DRRs for three patients (a) in-plane translation error (mm) (b) rotation error (degree)

registration error projected onto the femoral head ACS plane, while the out-of-plane error represents the registration error projected onto the vector from along the z-axis of the femoral head ACS plane. With the registration transformation between the sCT and the DRR acquired, the transformation between preoperative MRI and the DRR is calculated using Equation 2. For each MRI volume from each subject, the segmentation of the AVN lesion and the ideal drilling paths are annotated. The calculated transformation is used to re-project these annotations onto the original DRRs. The result is shown in Figure 9.

5. Discussion

The simulation study has shown promising results for the proposed registration pipeline to register the preoperative MRI and the 2D radiographs. In Figure 6, the gradient consistency integrated CycleGAN has shown to be a feasible method to perform style transfer from the MRI modality to the CT modality even with the limited training size, as we currently only have access to a total of three MRI volumes with small image spacing between the coronal planes. The generated sCT volumes preserve compact bone structures from the input MRI volumes and map them to a high CT intensity; while visible structures in MRI such as muscles, urinary bladder, and sciatic nerves are mapped to low intensities in the sCT. The registration result of the femur bone between the sCT and the DRR has a mean translation error of 12.95 $\pm$ 4.90 mm with a mean rotation error of 4.51 $\pm$ 2.67 degrees. The accuracy of the preoperative annotations on the intraoperative 2D radiographs is the same as the in-plane translation error acquired in Table 1, which has a mean of 4.55 $\pm$ 1.92 mm translation error and the same rotation registration error. As shown in Figure 10, the in-plane translation error in the first subject is slightly smaller than the other two subjects, while the rotation error remains similar among all three subjects. The left or right femur does not demonstrate a significant impact on the registration result.

In this experiment, the translation component of the registration error is a significant error for purposes such as robot-guided surgery, while a 2-mm error is considered to match the clinical requirement of core decompression (Wang et al. 2017). In this

Table 1.: Femur registration error between sCT and DRR. "S1", "S2", "S3" are the three patients in this study. "l" and "r" are the abbreviation of the left and right femur, respectively.

		Translation error (mm)			Rotation error (degree)			
		out-of-plane	in-plane	total	x	y	z	total
S1	l	8.25±1.91	2.73±1.33	8.81±1.77	1.62±1.03	1.00±0.64	2.59±1.79	3.43±1.76
	r	8.56±1.65	2.98±2.18	9.27±1.80	2.63±2.30	1.76±1.10	3.20±1.94	4.62±3.02
S2	l	9.75±2.13	5.75±2.48	11.52±2.32	3.86±2.24	2.43±1.82	4.13±1.44	6.36±2.75
	r	12.12±1.56	5.30±2.39	13.48±0.90	2.32±1.74	1.67±1.25	3.02±2.01	4.20±2.87
S3	l	11.49±1.62	5.94±1.40	13.02±1.37	2.25±1.46	1.43±1.09	3.23±1.75	4.31±2.28
	r	11.58±2.10	4.83±1.69	12.64±2.16	2.30±2.50	1.52±1.08	2.76±1.61	4.12±2.83
Average		10.29±1.80	4.55±1.92	12.95±4.90	2.50±1.99	1.63±1.24	3.15±1.76	4.51±2.67

study, the translation error mostly originates from the out-of-plane translation error and the less accurate sCT model used for registration. There are theoretical accuracy limitations in a shape matching process during registration as the estimated femur may be positioned closer or further to the camera along the z-axis of the femoral ACS frame (Fregly et al. 2005). Since slight movement along this axis maintains the projected shape of the femur in sCT, it has a smaller impact on the calculation of similarity scores during registration, which leads to low rotation registration errors but less ideal translation registration results.

Another source of the translation error may come from the sCT segmentation. Since the sCT is generated from the CycleGAN-based network with limited training size, the border of the proximal femur in the sCT may be affected by the soft tissues in the MRI and become less accurate. An example is shown in Figure 8, where the geometry of the sCT femur projections mostly align with the DRRs except for the greater trochanter of the femur. This misalignment may have a negative impact during the optimization step in registration. The issue could be mitigated by increasing CycleGAN training samples or by implementing additional loss functions that enhance the gradient consistency. Due to the lack of distinct features of the proximal femur in the DRRs, Gao et al. have proposed a two-step registration where the pelvis is first registered for a better femoral pose initialization since the pelvis has a rich collection of distinct features that leads to accurate registration accuracy (Gao et al. 2020). Our future work will extend the current registration pipeline to integrate the two-step registration and include multi-view registration for better registration translation accuracy.

Although the translation registration error in out-of-plane direction needs to be improved for clinical applications, the 4.55 ± 1.92 mm in-plane translation error and the 4.51 ± 2.67 degree rotation error acquired in this study ensure that the projection of the sCT is positionally close to the target on the 2D imaging plane. The accuracy in the imaging plane is critical when overlaying the segmented preoperative lesion segmentation or planned drilling paths onto the radiographs. For a common core-decompression surgery where a 6-10 mm cylindrical drill is used, we believe the overlay accuracy will provide a good intraoperative visual guidance for the surgeons (Pierce et al. 2015b), and the accuracy may further improve once the multi-step and multi-view registration is integrated. An example of the overlay is shown in Figure 9, where the 2D annotations of the preoperatively planned drilling trajectory and AVN lesions annotations are not visually affected by the out-of-plane translation errors. Although the experiment carried out in this paper is restricted to core decompression procedures, no assumptions were made that would preclude the application of the proposed registration pipeline to other surgical procedures.

Our registration pipeline solves for the transformation between preoperative MRI and intraoperative radiographs. The proposed pipeline is semi-automatic. The landmarks of the MRI and the CT have to be manually annotated by a clinician, which is essential for the construction of the femoral ACS and the initialization of the registration and the CT segmentation method occasionally requires manual touch up, while the remaining process is completed automatically. In this work, we have demonstrated the feasibility of cross-modality registration that has not been investigated in depth in previous studies. We aim to improve the pipeline by carrying out cadaver studies where a series of intraoperative C-arm fluoroscopy is collected and rigidly registered to the sCTs generated from preoperative MRI volumes, which completely remove the requirement of preoperative CT scans for core decompression surgeries.

6. Conclusion

In this work, we propose a novel 2D/3D registration pipeline to register preoperative MRI and intraoperative fluoroscopic images. To evaluate the feasibility of the proposed framework, we use a CycleGAN network to generate synthetic CT from MRI volumes and perform 2D/3D registration using digitally reconstructed fluoroscopic images. The experiment results show that the proposed registration pipeline achieves reasonable transformation between MRI and digitally reconstructed fluoroscopic images. Although this work uses the core decompression procedure as a surgical example, the proposed pipeline could be used to visualize preoperative annotations of segmented bone defects and medical instrument paths on the intraoperative fluoroscopic images. With the improved intraoperative visualization of bone defects, the proposed registration pipeline could improve the performance of surgical procedures and potentially reduce the number of fluoroscopic images required during surgery.

Acknowledgement

This work was partially supported by NIH grants R01EB023939 and R01EB016703 and in part by a collaborative research agreement with the Multi-Scale Medical Robotics Center in Hong Kong. The funding agency had no role in the study design, data collection, analysis of the data, writing of the manuscript, or the decision to submit the manuscript for publication.

References

Andreasen D, Edmund JM, Zografos V, Menze BH, Van Leemput K. 2016. Computed tomography synthesis from magnetic resonance images in the pelvis using multiple random forests and auto-context features. SPIE Proceedings.

Avants BB, Tustison NJ, Stauffer M, Song G, Wu B, Gee JC. 2014. The insight toolkit image registration framework. Frontiers in Neuroinformatics. 8.

Beckmann J, Goetz J, Baethis H, Kalteis T, Grifka J, Perlick L. 2006. Precision of computer-assisted core decompression drilling of the femoral head. Archives of Orthopaedic and Trauma Surgery. 126(6):374–379.

Brou Boni KN, Klein J, Vanquin L, Wagner A, Lacornerie T, Pasquier D, Reynaert N. 2020. Mr to ct synthesis with multicenter data in the pelvic area using a conditional generative adversarial network. Physics in Medicine amp; Biology. 65(7):075002.

Chang G, Boone S, Martel D, Rajapakse CS, Hallyburton RS, Valko M, Honig S, Regatte RR. 2017. Mri assessment of bone structure and microarchitecture. Journal of Magnetic Resonance Imaging. 46(2):323–337.

Chung WJ, Chung HW, Shin MJ, Lee SH, Lee MH, Lee JS, Kim MJ, Lee WK. 2012. Mri to differentiate benign from malignant soft-tissue tumours of the extremities: A simplified systematic imaging approach using depth, size and heterogeneity of signal intensity. The British Journal of Radiology. 85(1018).

Domb BG, Carreira DS. 2013. Endoscopic repair of full-thickness gluteus medius tears. Arthroscopy Techniques. 2(2).

Fregly BJ, Rahman HA, Banks SA. 2005. Theoretical accuracy of model-based shape matching for measuring natural knee kinematics with single-plane fluoroscopy. Journal of Biomechanical Engineering. 127(4):692–699.

Fu J, Singhrao K, Cao M, Yu V, Santhanam AP, Yang Y, Guo M, Raldow AC, Ruan D, Lewis JH, et al. 2020. Generation of abdominal synthetic cts from 0.35t mr images using generative adversarial networks for mr-only liver radiotherapy. Biomedical Physics amp; Engineering Express. 6(1):015033.

Gao C, Farvardin A, Grupp RB, Bakhtiarinejad M, Ma L, Thies M, Unberath M, Taylor RH, Armand M. 2020. Fiducial-free 2d/3d registration for robot-assisted femoroplasty. IEEE Transactions on Medical Robotics and Bionics. 2(3):437–446.

García E, Diez Y, Diaz O, Lladó X, Gubern-Mérida A, Martí R, Martí J, Oliver A. 2019. Breast mri and x-ray mammography registration using gradient values. Medical Image Analysis. 54:76–87.

Geisert WC, Perdue AM, Ozer K. 2017. Osseoscopy: Direct visualization to assist core decompression and debridement of necrotic bone defects. Arthroscopy Techniques. 6(3).

Goodfellow I, Pouget-Abadie J, Mirza M, Xu B, Warde-Farley D, Ozair S, Courville A, Bengio Y. 2014. Generative adversarial nets. In: Ghahramani Z, Welling M, Cortes C, Lawrence N, Weinberger K, editors. Advances in Neural Information Processing Systems; vol. 27. Curran Associates, Inc.

Grupp RB, Armand M, Taylor RH. 2018. Patch-based image similarity for intraoperative 2d/3d pelvis registration during periacetabular osteotomy. Lecture Notes in Computer Science:153–163.

Grupp RB, Hegeman RA, Murphy RJ, Alexander CP, Otake Y, McArthur BA, Armand M, Taylor RH. 2020. Pose estimation of periacetabular osteotomy fragments with intraoperative x-ray navigation. IEEE Transactions on Biomedical Engineering. 67(2):441–452.

Hansen N, Müller SD, Koumoutsakos P. 2003. Reducing the time complexity of the derandomized evolution strategy with covariance matrix adaptation (cma-es). Evolutionary Computation. 11(1):1–18.

Hiasa Y, Otake Y, Takao M, Matsuoka T, Takashima K, Carass A, Prince JL, Sugano N, Sato Y. 2018. Cross-modality image synthesis from unpaired data using cyclegan. Simulation and Synthesis in Medical Imaging:31–41.

Kalantar R, Messiou C, Winfield JM, Renn A, Latifoltojar A, Downey K, Sohaib A, Lalondrelle S, Koh DM, Blackledge MD, et al. 2021. Ct-based pelvic t1-weighted mr image synthesis using unet, unet++ and cycle-consistent generative adversarial network (cycle-gan). Frontiers in Oncology. 11.

Krčah M, Székely G, Blanc R. 2011. Fully automatic and fast segmentation of the femur bone from 3d-ct images with no shape prior. In: 2011 IEEE International Symposium on Biomedical Imaging: From Nano to Macro. p. 2087–2090.

Leynes AP, Yang J, Wiesinger F, Kaushik SS, Shanbhag DD, Seo Y, Hope TA, Larson PE. 2017. Zero-echo-time and dixon deep pseudo-ct (zedd ct): Direct generation of pseudo-ct images for pelvic pet/mri attenuation correction using deep convolutional neural networks with multiparametric mri. Journal of Nuclear Medicine. 59(5):852–858.

Lieberman JR. 2004. Core decompression for osteonecrosis of the hip. Clinical Orthopaedics and Related Research. 418:29–33.

Malizos KN, Karantanas AH, Varitimidis SE, Dailiana ZH, Bargiotas K, Maris T. 2007. Os-

teonecrosis of the femoral head: Etiology, imaging and treatment. European Journal of Radiology. 63(1):16–28.
Mertzanidou T, Hipwell J, Cardoso MJ, Zhang X, Tanner C, Ourselin S, Bick U, Huisman H, Karssemeijer N, Hawkes D, et al. 2012. Mri to x-ray mammography registration using a volume-preserving affine transformation. Medical Image Analysis. 16(5):966–975.
Nascimento D, Suchard G, Hatem M, de Abreu A. 2014. The role of magnetic resonance imaging in the evaluation of bone tumours and tumour-like lesions. Insights into Imaging. 5(4):419–440.
Nie D, Trullo R, Lian J, Wang L, Petitjean C, Ruan S, Wang Q, Shen D. 2018. Medical image synthesis with deep convolutional adversarial networks. IEEE Transactions on Biomedical Engineering. 65(12):2720–2730.
Nolte LP, Slomczykowski MA, Berlemann U, Strauss MJ, Hofstetter R, Schlenzka D, Laine T, Lund T. 2000. A new approach to computer-aided spine surgery: Fluoroscopy-based surgical navigation. European Spine Journal. 9(S1).
Nori M. 2015. Mri evaluation of post core decompression changes in avascular necrosis of hip. Journal of Clinical and Diagnostic Research.
Pierce TP, Jauregui JJ, Cherian JJ, Elmallah RK, Mont MA. 2015a. Imaging evaluation of patients with osteonecrosis of the femoral head. Current Reviews in Musculoskeletal Medicine. 8(3):221–227.
Pierce TP, Jauregui JJ, Elmallah RK, Lavernia CJ, Mont MA, Nace J. 2015b. A current review of core decompression in the treatment of osteonecrosis of the femoral head. Current Reviews in Musculoskeletal Medicine. 8(3):228–232.
Rocchi M, Del Piccolo N, Mazzotta A, Giavaresi G, Fini M, Facchini F, Stagni C, Dallari D. 2020. Core decompression with bone chips allograft in combination with fibrin platelet-rich plasma and concentrated autologous mesenchymal stromal cells, isolated from bone marrow: Results for the treatment of avascular necrosis of the femoral head after 2 years minimum follow-up. HIP International. 30:3–12.
Rusinkiewicz S, Levoy M. 2001. Efficient variants of the icp algorithm. In: Proceedings Third International Conference on 3-D Digital Imaging and Modeling. p. 145–152.
Saini A, Saifuddin A. 2004. Mri of osteonecrosis. Clinical Radiology. 59(12):1079–1093.
Talmaç MA. 2018. The results of core decompression treatment in femoral head avascular necrosis. SiSli Etfal Hastanesi Tip Bulteni / The Medical Bulletin of Sisli Hospital.
Tian R, Luo S, Wang C, Wang K, Yang P. 2021. Robot-assisted core decompression combined with bone grafting can improve the early clinical results in femoral head necrosis: A prospective cohort study.
van der Bom MJ, Pluim JP, Gounis MJ, van de Kraats EB, Sprinkhuizen SM, Timmer J, Homan R, Bartels LW. 2011. Registration of 2d x-ray images to 3d mri by generating pseudo-ct data. Physics in Medicine and Biology. 56(4):1031–1043.
Veillette CJ, Mehdian H, Schemitsch EH, McKee MD. 2006. Survivorship analysis and radiographic outcome following tantalum rod insertion for osteonecrosis of the femoral head. Journal of Bone and Joint Surgery. 88:48–55.
Wang W, Hu W, Yang P, Dang XQ, Li XH, Wang KZ. 2017. Patient-specific core decompression surgery for early-stage ischemic necrosis of the femoral head. PLOS ONE. 12(5).
Yang H, Sun J, Carass A, Zhao C, Lee J, Prince JL, Xu Z. 2020. Unsupervised mr-to-ct synthesis using structure-constrained cyclegan. IEEE Transactions on Medical Imaging. 39(12):4249–4261.
Yu X, Zhang D, Chen X, Yang J, Shi L, Pang Q. 2018. Effectiveness of various hip preservation treatments for non-traumatic osteonecrosis of the femoral head: A network meta-analysis of randomized controlled trials. Journal of Orthopaedic Science. 23(2):356–364.
Zhang X, Zheng G, Langlotz F, Nolte L. 2006. Assessment of spline-based 2d–3d registration for image-guided spine surgery. Minimally Invasive Therapy amp; Allied Technologies. 15(3):193–199.
Zhu JY, Park T, Isola P, Efros AA. 2017. Unpaired image-to-image translation using cycle-consistent adversarial networks. 2017 IEEE International Conference on Computer Vision.